ACCURACY OF HEMP CODE SOLUTIONS

Robert R. Karpp

Ballistic Research Laboratories
Aberdeen Proving Ground, Maryland

January 1973

BRL MR 2268

BRL

AD

MEMORANDUM REPORT NO. 2268

ACCURACY OF HEMP CODE SOLUTIONS

by

Robert R. Karpp

January 1973

USA BALLISTIC RESEARCH LABORATORIES
ABERDEEN PROVING GROUND, MARYLAND

Destroy this report when it is no longer needed.
Do not return it to the originator.

Secondary distribution of this report by originating or sponsoring activity is prohibited.

Additional copies of this report may be purchased from the U.S. Department of Commerce, National Technical Information Service, Springfield, Virginia 22151

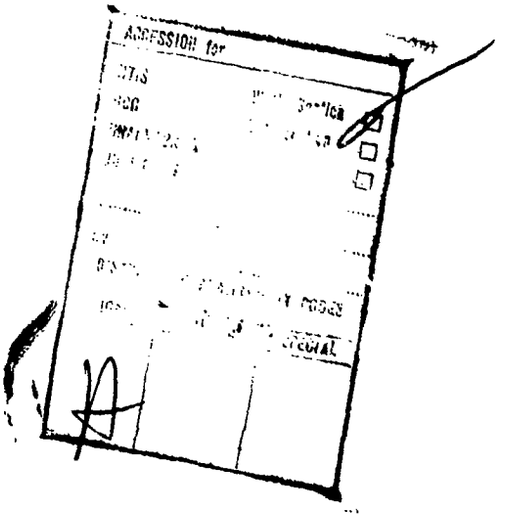

The findings in this report are not to be construed as an official Department of the Army position, unless so designated by other authorized documents.

UNCLASSIFIED
Security Classification

DOCUMENT CONTROL DATA - R & D

(Security classification of title, body of abstract and indexing annotation must be entered when the overall report is classified)

1. ORIGINATING ACTIVITY (Corporate author)	2a. REPORT SECURITY CLASSIFICATION
U.S. Army Ballistic Research Laboratories Aberdeen Proving Ground, Maryland 21005	UNCLASSIFIED
	2b. GROUP

3. REPORT TITLE

ACCURACY OF HEMP CODE SOLUTIONS

4. DESCRIPTIVE NOTES (Type of report and inclusive dates)

Memorandum Report

5. AUTHOR(S) (First name, middle initial, last name)

ROBERT R. KARPP

6. REPORT DATE	7a. TOTAL NO. OF PAGES	7b. NO. OF REFS
JANUARY 1973	45 42	6

8a. CONTRACT OR GRANT NO.	9a. ORIGINATOR'S REPORT NUMBER(S)
b. PROJECT NO. 1T061102A33E	MEMORANDUM REPORT NO. 2268
c.	9b. OTHER REPORT NO(S) (Any other numbers that may be assigned this report)
d.	

10. DISTRIBUTION STATEMENT

Approved for public release; distribution unlimited.

11. SUPPLEMENTARY NOTES	12. SPONSORING MILITARY ACTIVITY
	U.S. Army Materiel Command Washington, DC 20315

13. ABSTRACT

Results of HEMP code calculations of simple problems are compared with exact results to determine the accuracy with which this numerical technique solves initial-boundary value problems. More complicated problems of metal liners accelerated by explosives were also calculated with this code, and these results were compared with experimental results to determine how well the code simulates these physical processes. It is concluded that HEMP calculations are accurate enough to be useful as a tool for predicting the gross motion of metals accelerated by detonating explosives.

DD FORM 1 NOV 68 1473 REPLACES DD FORM 1473, 1 JAN 64, WHICH IS OBSOLETE FOR ARMY USE.

UNCLASSIFIED
Security Classification

14. KEY WORDS	LINK A		LINK B		LINK C	
	ROLE	WT	ROLE	WT	ROLE	WT
Numerical Solutions of P.D.E.						
Explosive-Metal Interactions						
Computer aided warhead design						

BALLISTIC RESEARCH LABORATORIES

MEMORANDUM REPORT NO. 2268

JANUARY 1973

ACCURACY OF HEMP CODE SOLUTIONS

Robert R. Karpp

RDT&E Project No. 1T061102A33E

ABERDEEN PROVING GROUND, MARYLAND

B A L L I S T I C R E S E A R C H L A B O R A T O R I E S

MEMORANDUM REPORT NO. 2268

RKarpp/pac
Aberdeen Proving Ground, Md.
January 1973

ACCURACY OF HEMP CODE SOLUTIONS

ABSTRACT

Results of HEMP code calculations of simple problems are compared with exact results to determine the accuracy with which this numerical technique solves initial-boundary value problems. More complicated problems of metal liners accelerated by explosives were also calculated with this code, and these results were compared with experimental results to determine how well the code simulates these physical processes. It is concluded that HEMP calculations are accurate enough to be useful as a tool for predicting the gross motion of metals accelerated by detonating explosives.

TABLE OF CONTENTS

LIST OF ILLUSTRATIONS

LIST OF ILLUSTRATIONS

I. INTRODUCTION

The HEMP[1]* code is a computer program which is formulated to approximately solve the conservation equations of mass, momentum, and energy subject to appropriate initial and boundary conditions. The materials under consideration are described as hydrodynamic materials (fluids) or elastic-perfectly plastic materials. An energy release routine which simulates the detonation of a high explosive is also included. This code contains the essential features necessary to solve explosive-metal acceleration problems which are relevant to the design of warheads. Since we plan to use this code to study and predict the performance of warheads, we first want to gain an understanding of the accuracy obtainable from it. Two important questions regarding the accuracy of finite-difference codes are: (1) how well does the numerical scheme solve the governing system of partial differential equations, and (2) how well do these equations model the physical process? To obtain some sort of answer to these questions, we first compared numerical solutions with exact solutions to simple problems, and then, for more complicated problems, we compared numerical solutions with experimental results.

In Section II, a sequence of simple problems which possess exact solutions is solved numerically with the code, and comparisons between the exact and approximate solutions are made. Problems involving perfect fluids, elastic solids, elastic-plastic solids, and detonating explosives were considered.

In Section III, comparisons between experimental test results and HEMP code calculations are made for explosive-metal systems. Conclusions from these comparisons are presented in Section IV. Although the

**References are listed on page 35.*

problem formulation and method of solution used in the HEMP code have been documented by the originators[1,2], a very brief outline of the formulation is presented, for completeness, in Appendix A.

II. HEMP SOLUTIONS COMPARED WITH EXACT RESULTS

In this section, the results of HEMP calculations applied to a series of simple problems are presented. For these problems, the exact solutions are well known and can easily be evaluated. These exact solutions are then compared with the HEMP results in order to determine how well the governing equations are satisfied by the HEMP solutions.

As a first illustration, the problem of a high pressure, ideal gas initially trapped in a tube and then released was calculated with three different mesh sizes. The results are illustrated in Figure 1. For this and subsequent figures, the notation (P) pressure, (ρ) density, (e) specific internal energy, (γ) a constant, (G) shear modulus, (σ_y) yield strength in tension, and (Vo) initial velocity is used. The solid line on the pressure-position graph indicates the exact solution at 10 μsec after release of the gas, and the three numerical results are indicated by the points. As the number of points in the numerical mesh is increased the numerical solution approaches the exact solution, and convergence of the numerical scheme is indicated. All solutions represent the plane rarefaction wave reasonably well. The variation of properties across the tube, for the HEMP results, was negligible. For computational purposes, this one-dimensional problem can be generalized slightly by using a mesh which is initially skewed as shown in Figure 2. The plane rarefaction then passes obliquely across the zones, and, for computational purposes, the problem is two-dimensional. The numerical solution is degraded only slightly because of this two-dimensional effect, as indicated by the comparison between calculations with the rectangular and non-rectangular meshes shown in Figure 2. The most noticable result of the non-rectangular zoning appears in the position

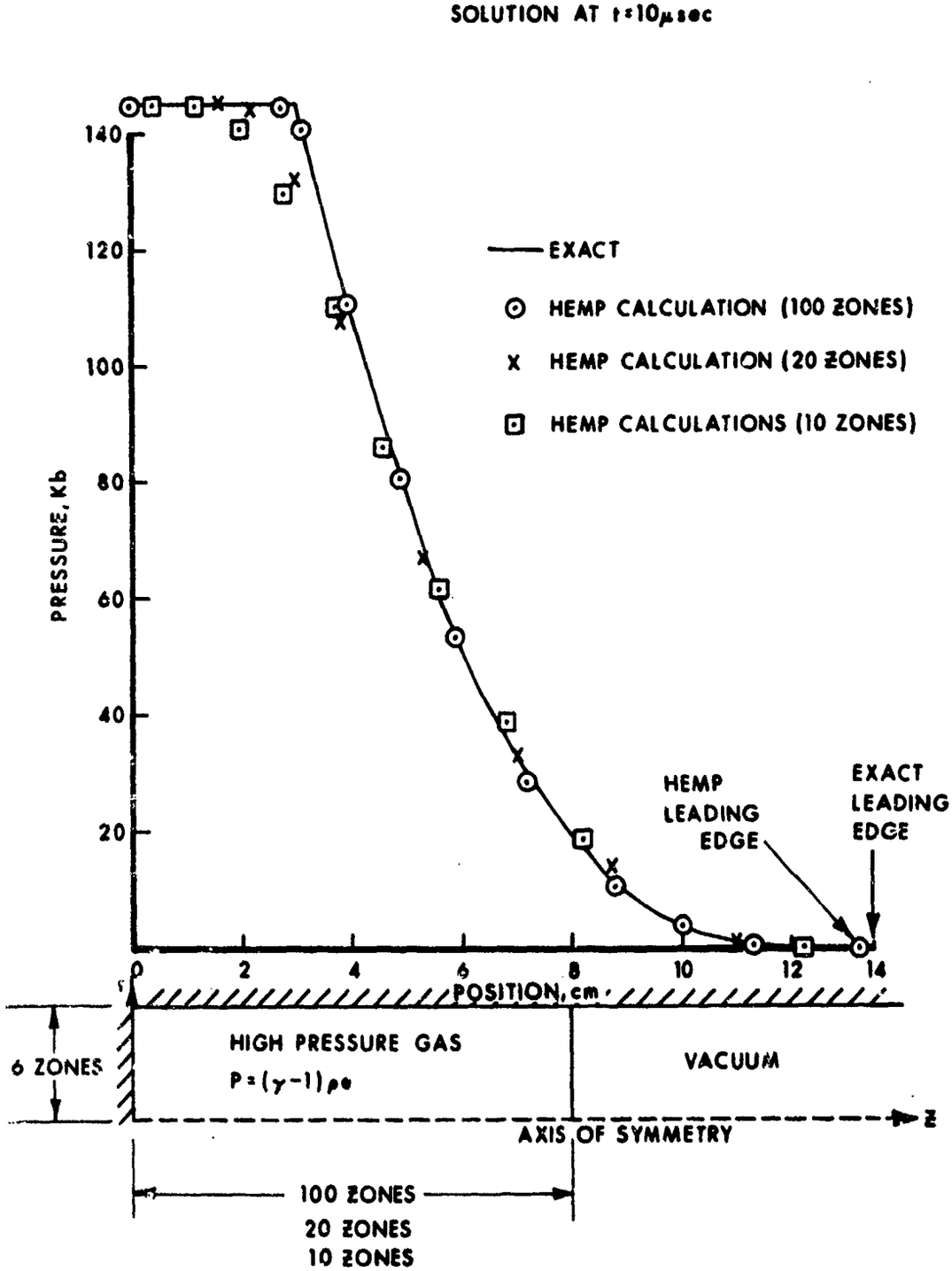

Figure 1. Numerical solution for the one-dimensional expansion of a high pressure gas using three different finite-difference zonings

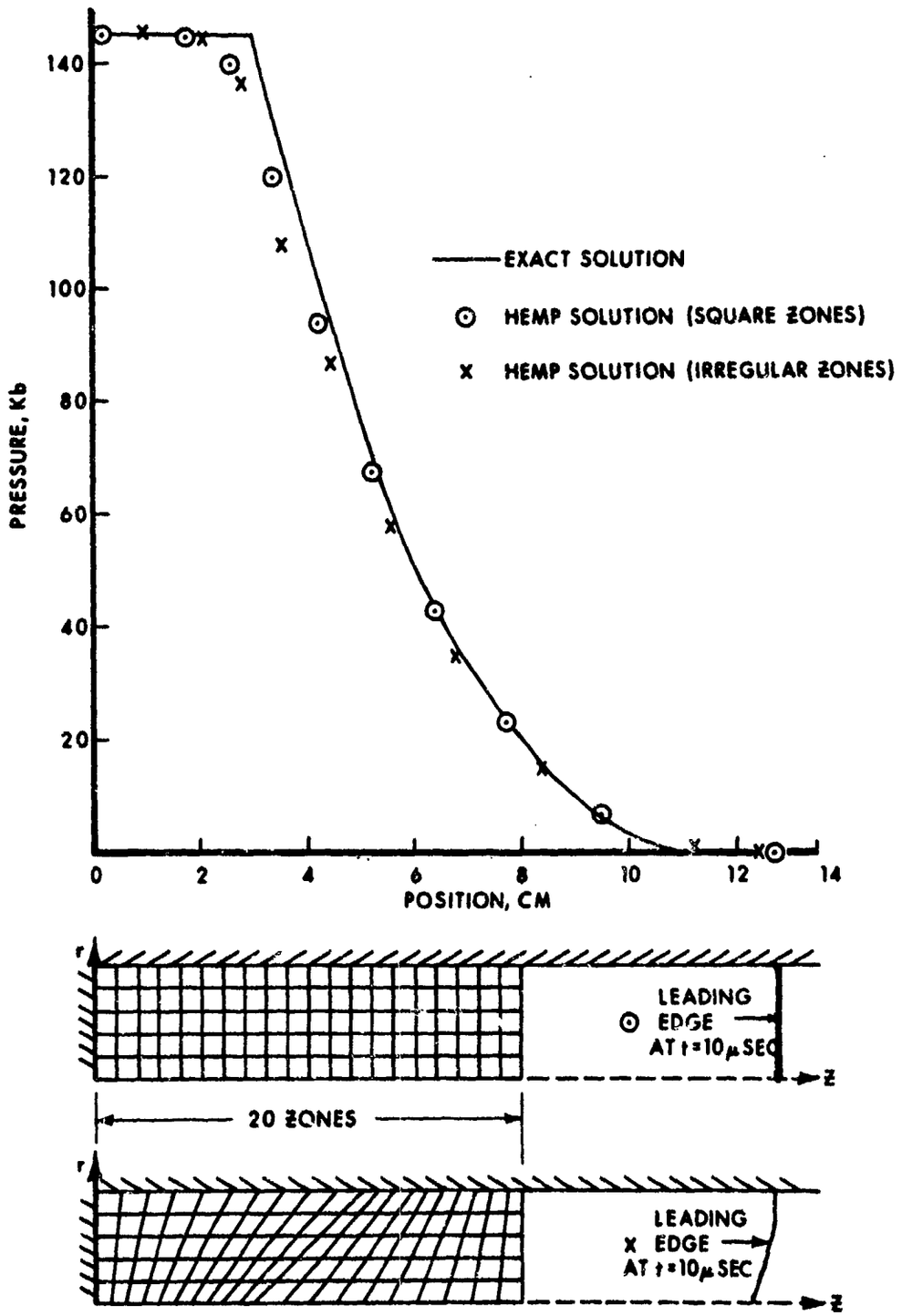

Figure 2. Effect of the initial zone shape upon the numerical solution of the gas expansion problem

of the gas boundary. However, for practical purposes, HEMP solutions appear to be reasonably accurate for expansion waves in an ideal gas.

Since an interest in the flow of metals also exists, a series of one-dimensional (uniaxial strain) impact problems was solved with the HEMP code. Figure 3 shows a typical Hugoniot curve (solid line) for an elastic-perfectly plastic material[3]. The dotted line indicates the straight line extension of the elastic portion of the Hugoniot. Three different wave structures, depending on the magnitude of the stress jump, can exist. If a stress jump of σ_1 is present, where σ_1 is below σ_Y, the yield point stress, an elastic wave with a single stress jump will be propagated. A double wave structure, elastic precursor followed by a plastic shock, will propagate if the stress jump is σ_2, where σ_2 is a stress above the yield point value but below the intersection of the dotted line with the Hugoniot. A stress jump σ_3 above the intersection point will again result in a single stress jump (shock).

The numerically calculated pressure distribution resulting from the elastic impact of two identical blocks is shown in Figure 4 along with the exact solution. The zoning and initial conditions of the problem are also shown. Boundary conditions of no vertical velocity on the upper or lower surfaces were used in the numerical solution. The HEMP values oscillate somewhat ($\pm$ 6%) about the exact value of 8 Kb. A smoother solution to this impact problem may be obtained by increasing the number of zones and by inserting a transition zone to smooth the initial velocity discontinuity. Results of calculations with these changes are shown in Figure 5 along with the initial velocity distribution. The improvement in the quality of the solution, compared to the solution shown in Figure 4, is apparent. This problem may also be treated as a two-dimensional problem by introducing the non-rectangular zoning indicated in Figure 6. The degradation of the solution due to two-dimensional effects can be seen by comparing Figure 6 with Figure 4. The oscillation in the numerical solution for the non-rectangular zoning case has increased in amplitude by a factor of two over the one-dimensional case. However, the solution can be made smoother by using more zones. A

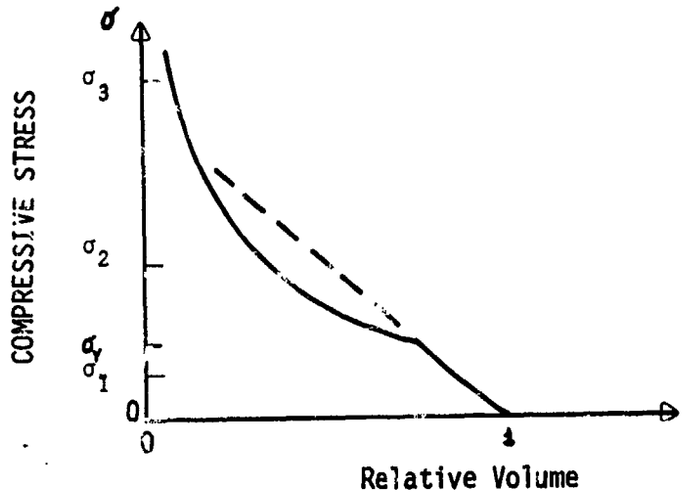

Figure 3. Schematic of a Hugoniot Curve for an Elastic - Plastic Material

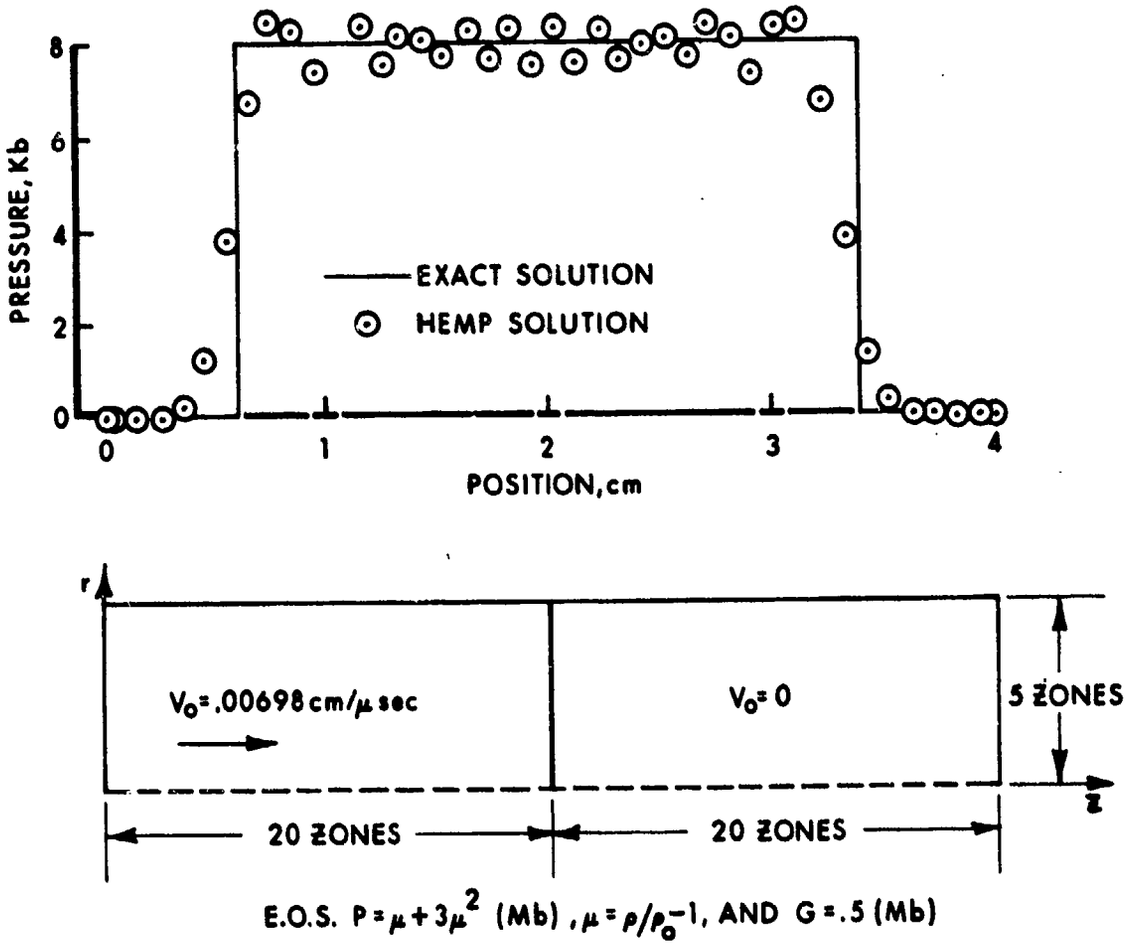

Figure 4. The initial configuration and pressure distribution 3 μsec after the one-dimensional impact of elastic blocks

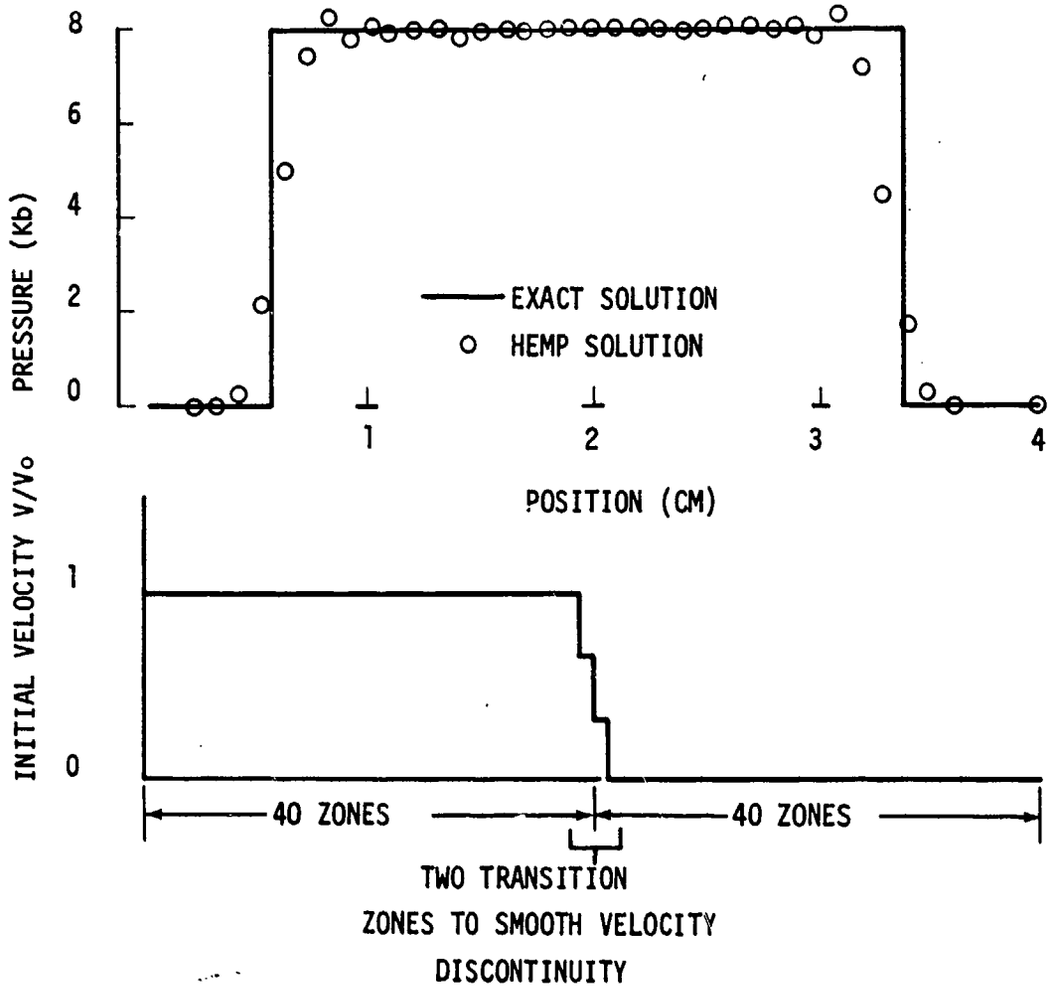

Figure 5. Improvement in the numerical solution of the elastic impact problem by using an initially fine zoning and a transition zone

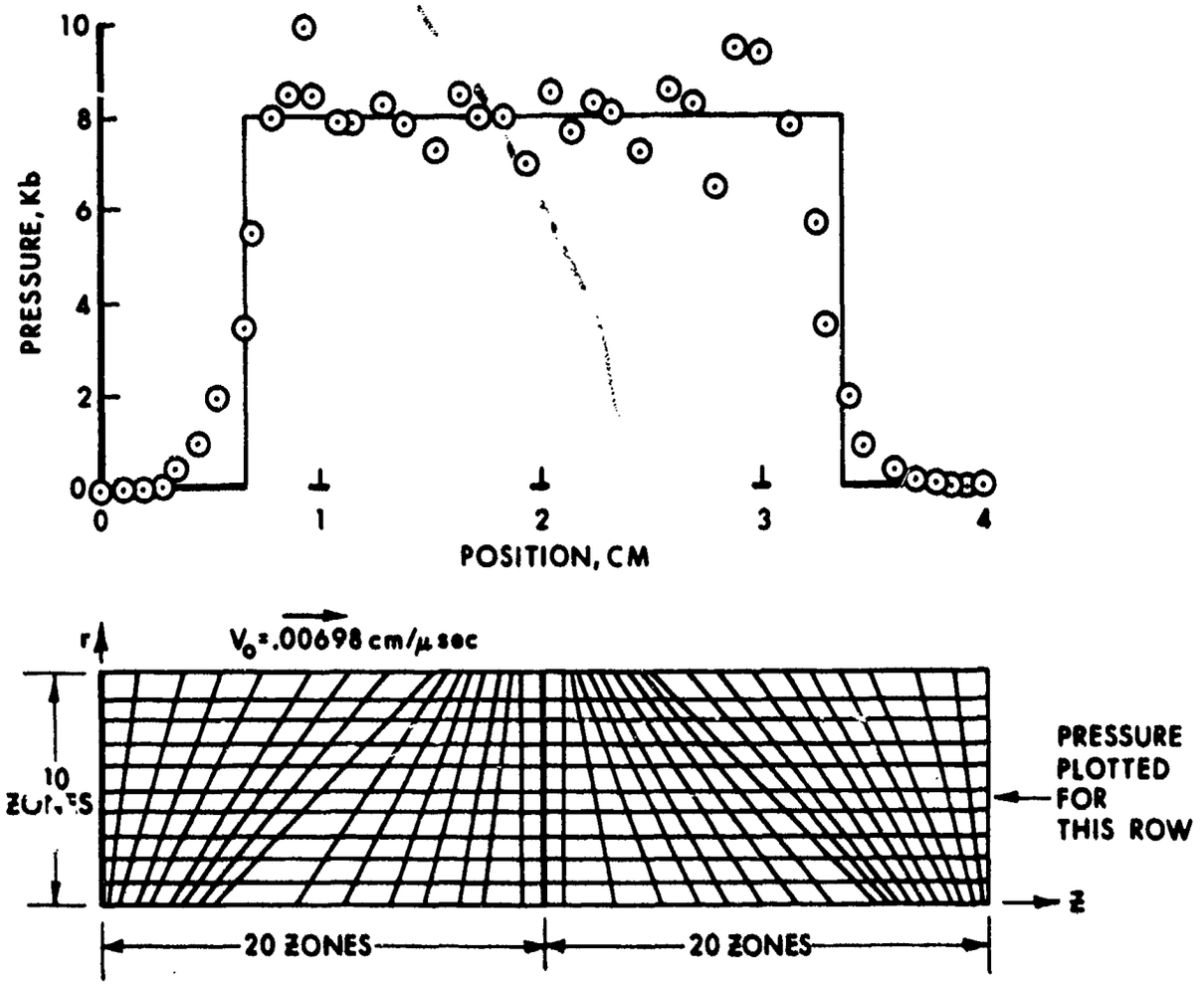

Figure 6. Effect of initial zone shape upon numerical solution of the elastic impact problem

numerical solution using 40 axial zones in the target material instead of 20 is shown in Figure 7 where both the pressure and particle velocity distribution are indicated. It has been suggested that oscillations in these solutions could be additionally reduced by introducing a linear artificial viscosity term[1].

If the impact velocity is sufficiently increased, the two wave structure, indicated by the stress level σ_2 of Figure 3, can be formed in the impacting materials. Figure 8 illustrates a part of the numerical solution for this case. If the impact velocity is further increased, the single wave structure, corresponding to the stress level σ_3, may be formed. The numerical results for this high velocity impact case are shown in Figure 9.

The conclusion from this series of impact problems is that the HEMP results do represent, within reasonable accuracy, the steady-state wave profiles which occur with the elastic-perfectly plastic material.

To simulate the detonation of a high explosive, an "explosive burn routine" is included in the code. The chemical energy released in the detonation process is stored in each zone as an initial internal energy. Release of this energy is started, in each zone, when the calculated position of the detonation reaches the zone center. To test this portion of the code, the problem of a one-dimensional Chapman-Jouquet (C-J) detonation wave propagating down a closed-end tube was numerically solved. Figure 10 shows the exact pressure distribution compared with two numerical solutions (100 zones and 20 zones). Both solutions fail to produce the peak pressure (C-J pressure). The peak pressure of the finely zoned solution is about 10% low. For this problem, the left boundary is fixed. If the left boundary is moved as a piston to the right with the C-J particle velocity, the peak pressure of the numerical solution does reproduce the exact C-J value for both zonings.

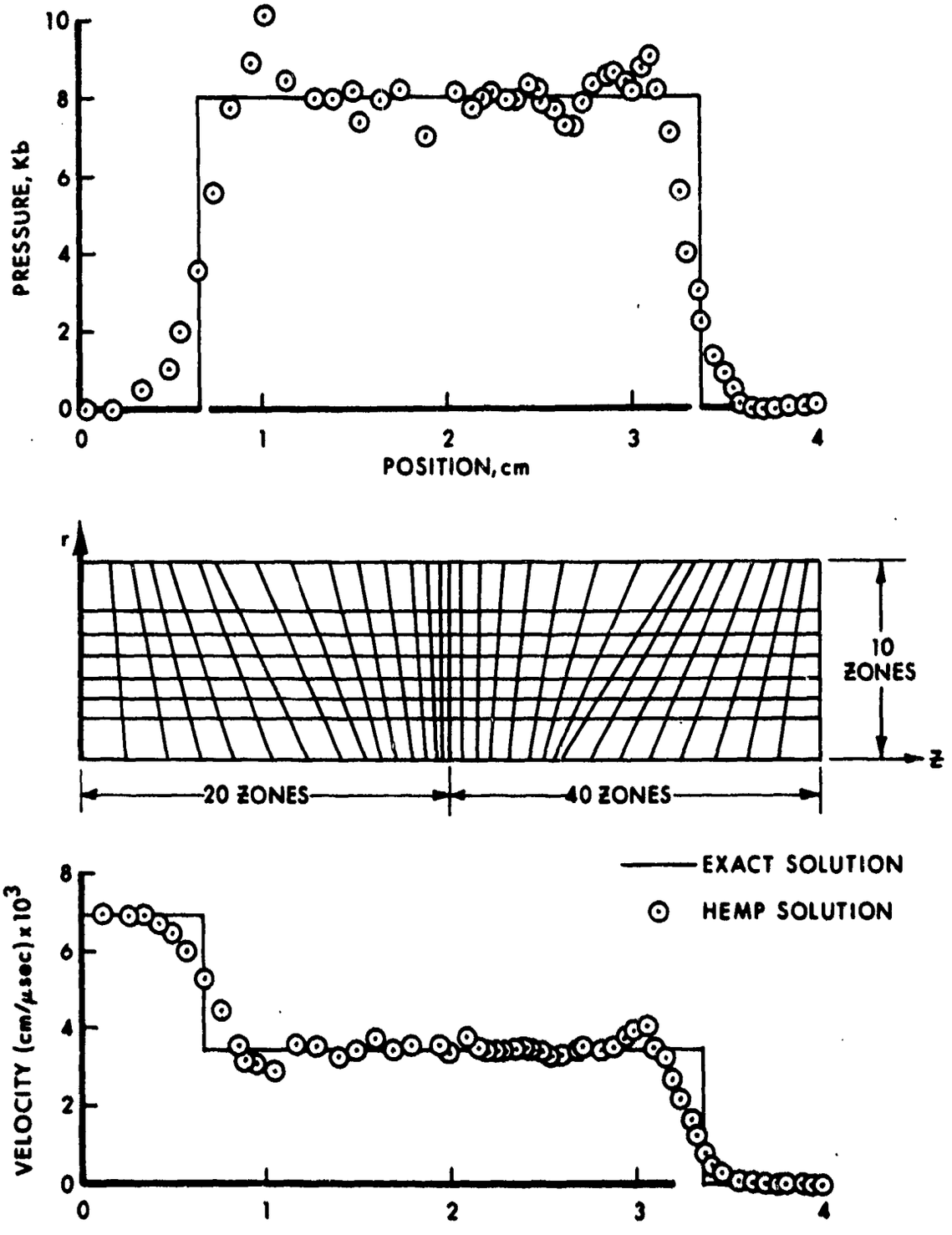

Figure 7. Improvement in the numerical solution of the elastic problem with skewed zones by refining the zoning

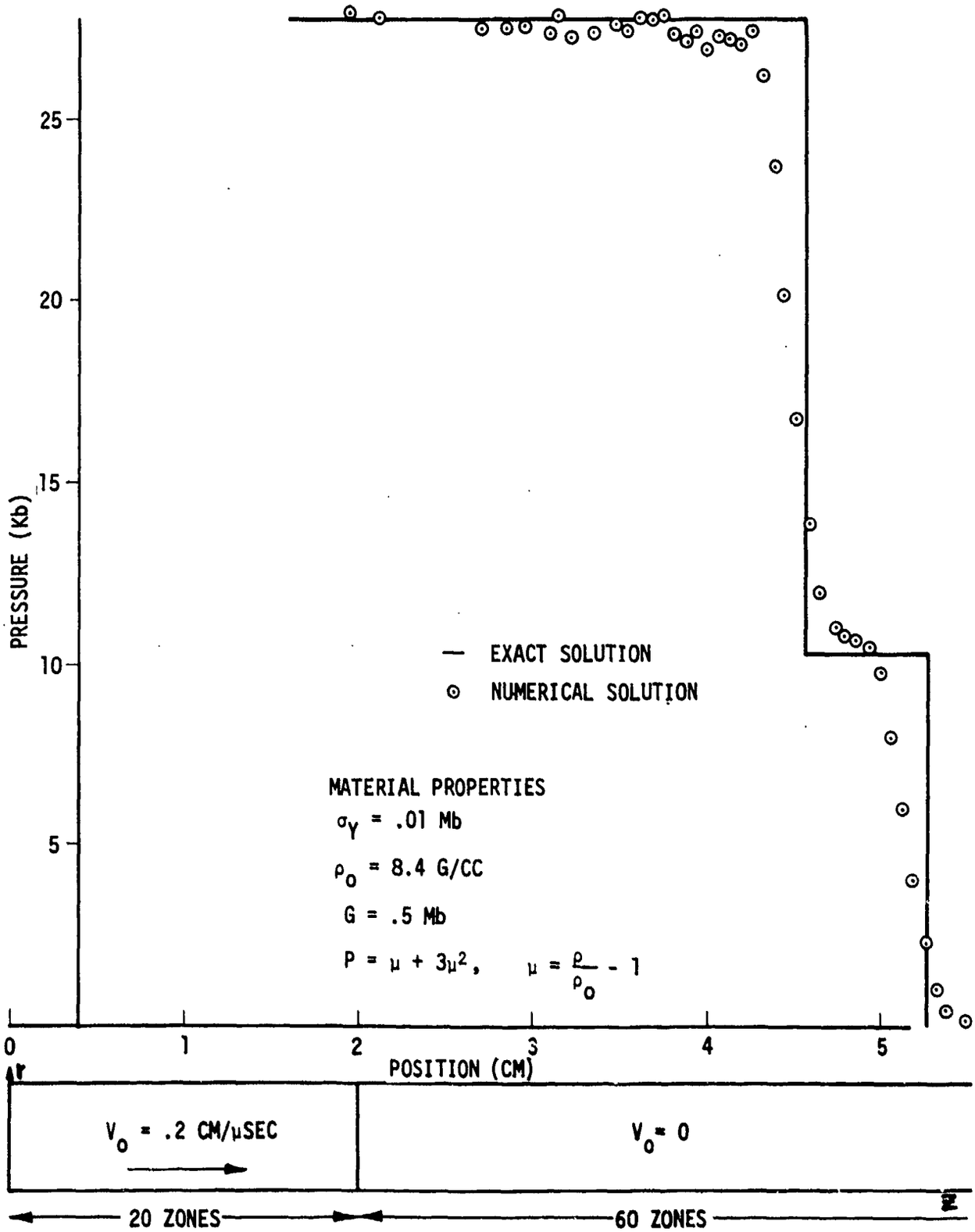

Figure 8. The numerical solution for the pressure distribution in the elastic-plastic wave resulting from one-dimensional impact

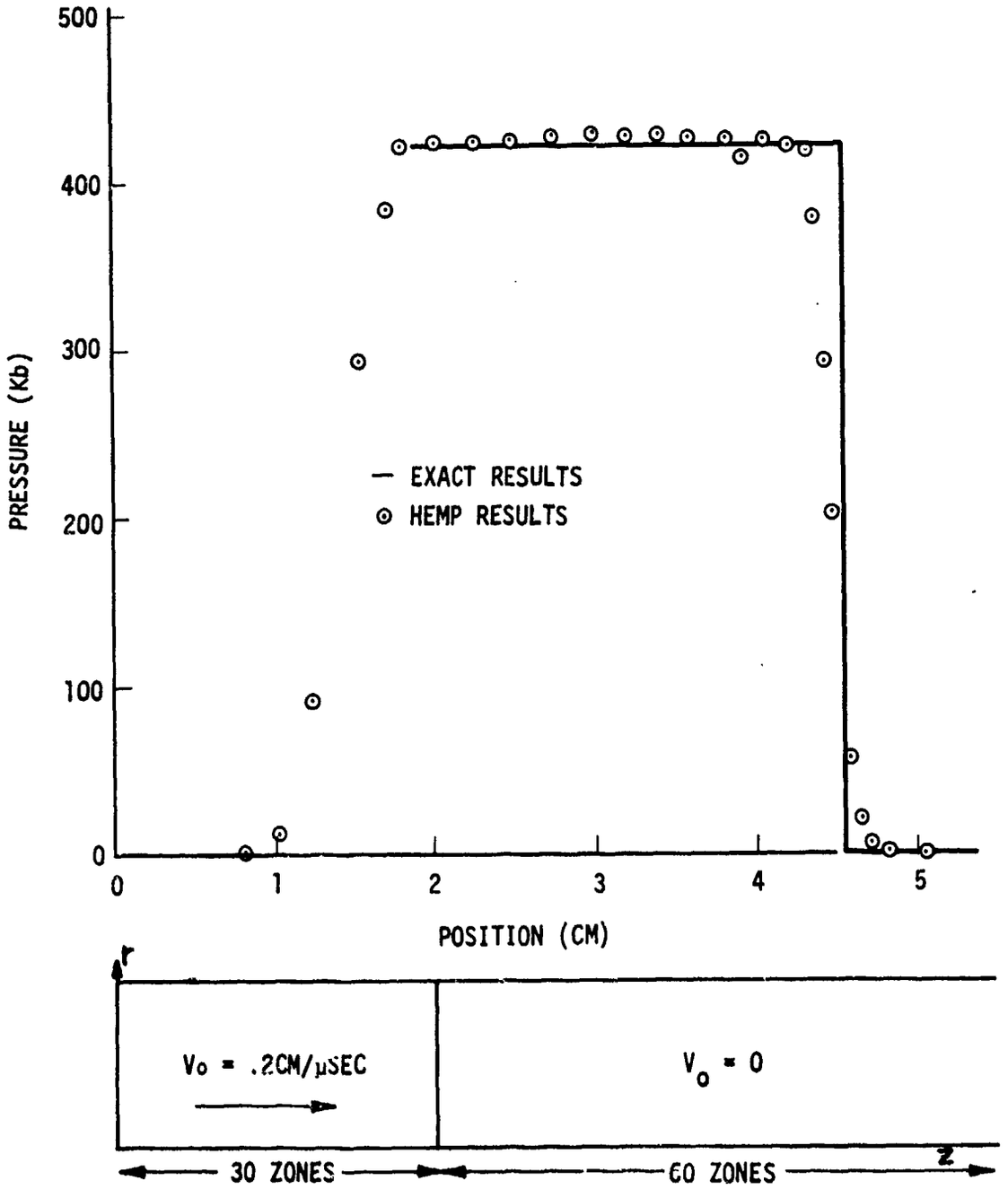

Figure 9.. The numerical solution for the pressure distribution resulting from high speed, one-dimensional impact

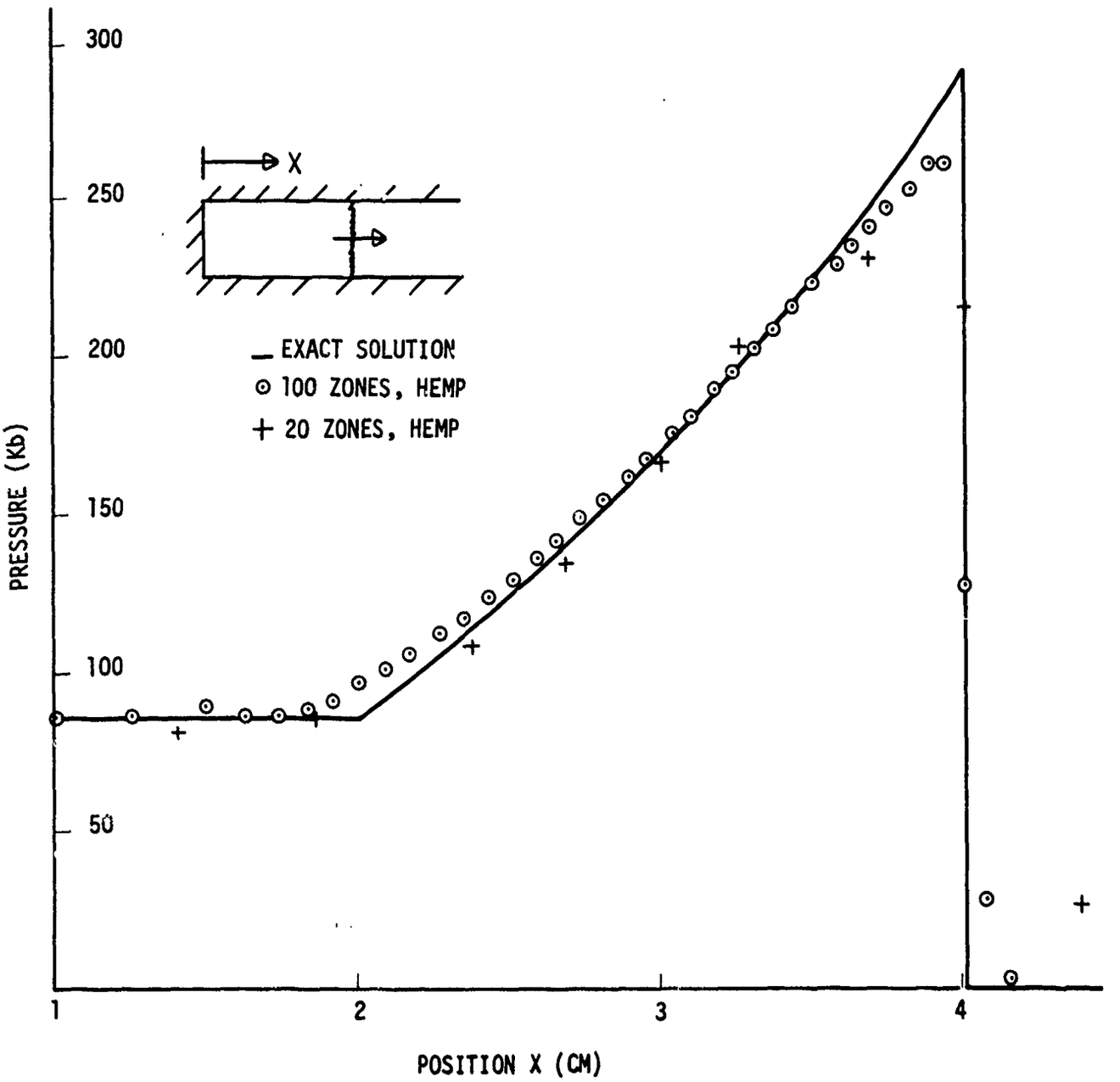

Figure 10. Calculated pressure distribution in a Chapman-Jouquet detonation wave with a fixed rear boundary (ref. 7)

III. HEMP SOLUTIONS COMPARED WITH EXPERIMENTAL RESULTS

The previous section demonstrated, for a few cases, the accuracy with which the code solves the partial differential equations and related jump conditions. In this section, the code calculations are compared with experimental results to determine the overall accuracy with which the code simulates the physical process of metal acceleration by explosive loading.

The problem of a cylindrical charge of explosive (Composition B) accelerating an aluminum disc was chosen for the first comparison. The experimental configuration as well as the experimental and numerical results are shown in Figure 11. Here, the motion of the free surface of the aluminum disc was measured as a function of time with a streak camera. The calculations were based on the JWL equation of state[4] for the explosive and an equation of state described by Wilkins[1] for the aluminum disc. The calculated results agree reasonably well with the experimental values (6 1/2% maximum error).

Figure 12 illustrates the results of a test which was designed to measure the terminal velocity of preformed steel fragments projected from the end of a Composition B charge. The experimental velocities were reported by Taylor[5]. The calculations were based on the JWL equation of state for Composition B and the equation of state which is incorporated in the code for iron. To model the preformed fragments, a hydrodynamic description (yield strength equal to zero) was used with the minimum pressure set at zero. The HEMP results duplicate the experimental values within about 6%. If one would use a Gurney type analysis to predict velocites for this configuration,[6] the predicted velocity would be about 2.8 mm/μsec, or a minimum error of about 32%.

A third comparison between calculated and experimental results is illustrated in Figures 13 and 14. A steel cylinder filled with Com-

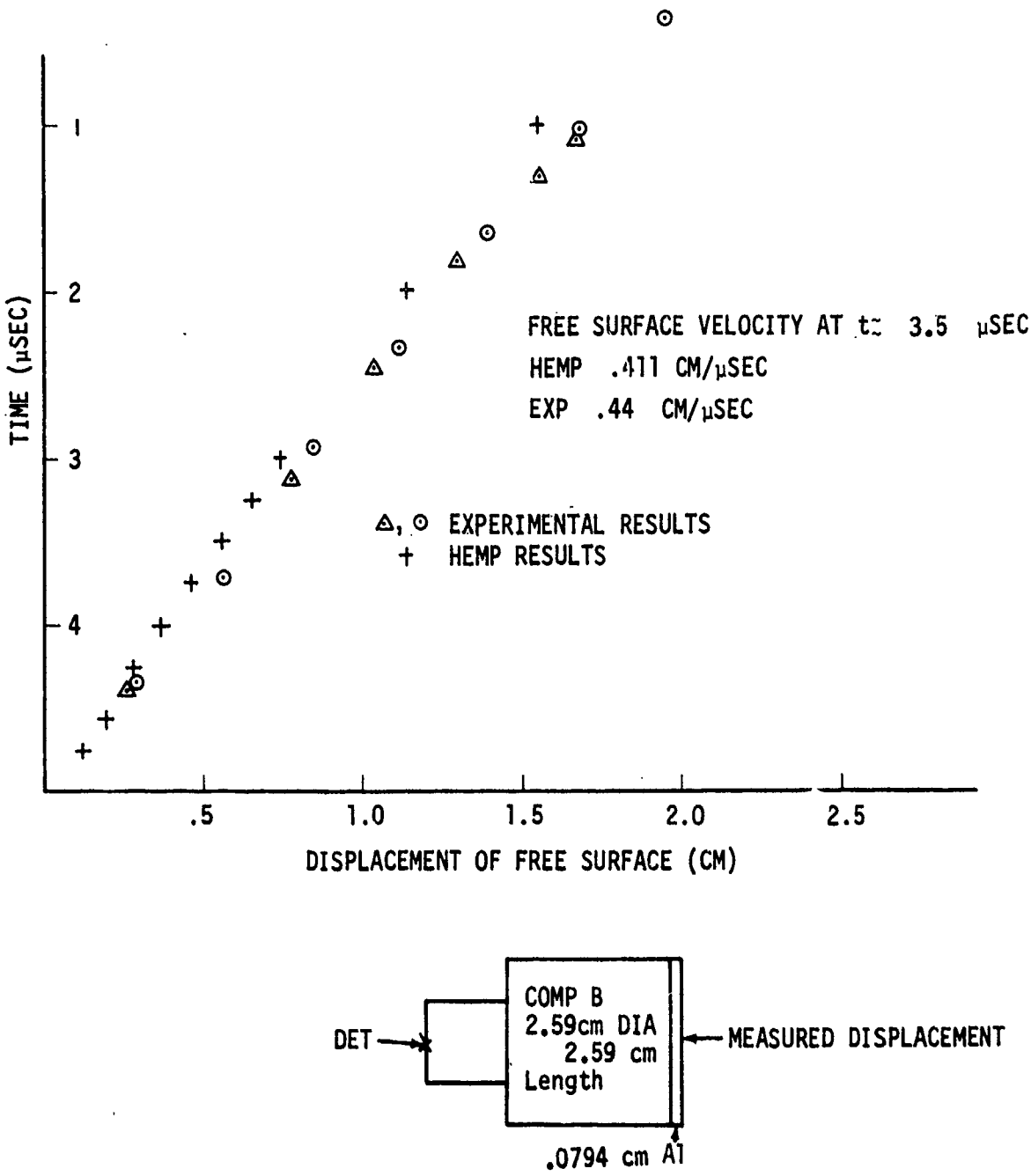

Figure 11. Calculated and experimental results for the acceleration of an aluminum disc propelled by a composition B explosive charge

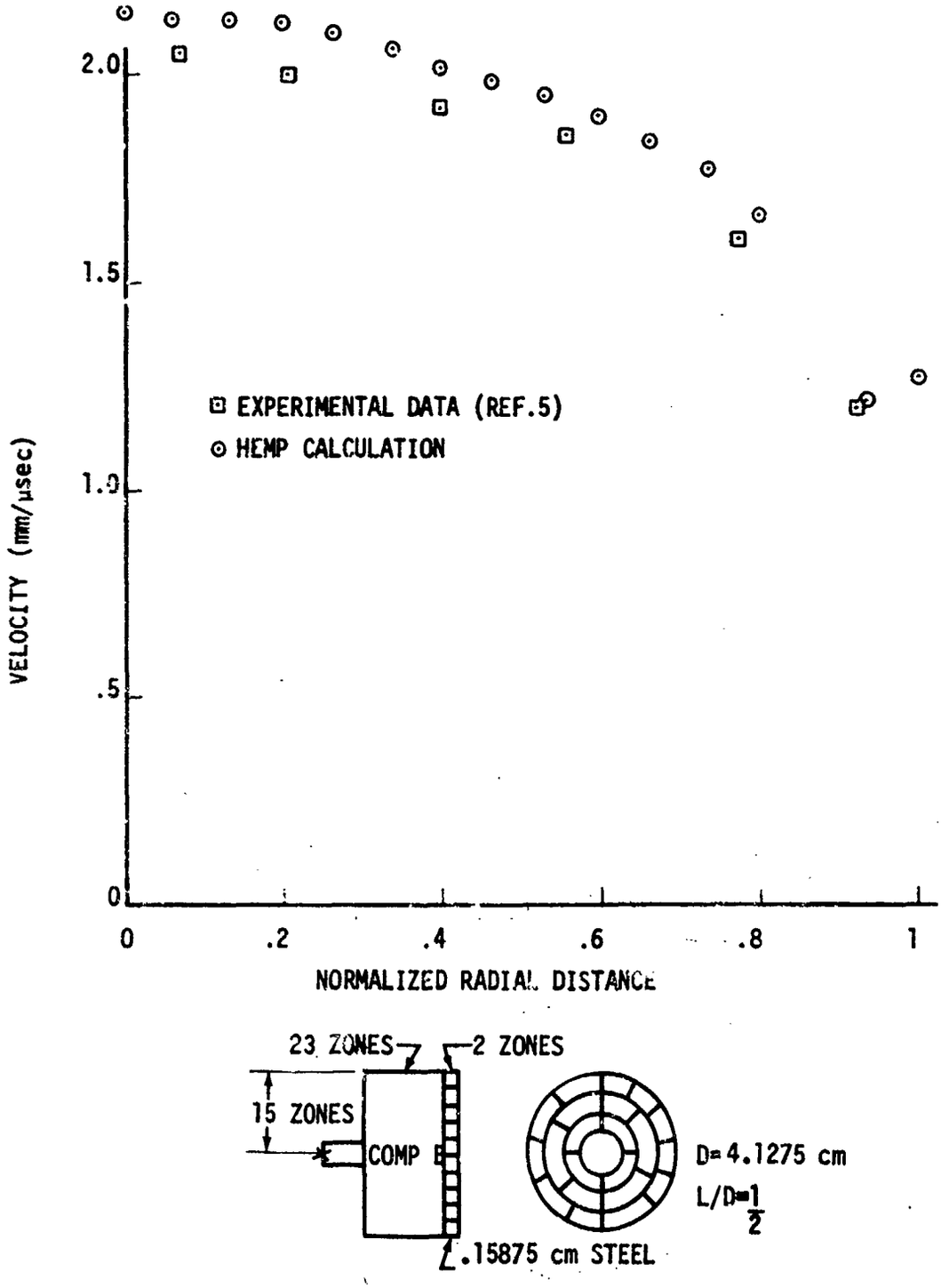

Figure 12. Calculated and experimental results for the acceleration of preformed fragments from the end of an explosive charge

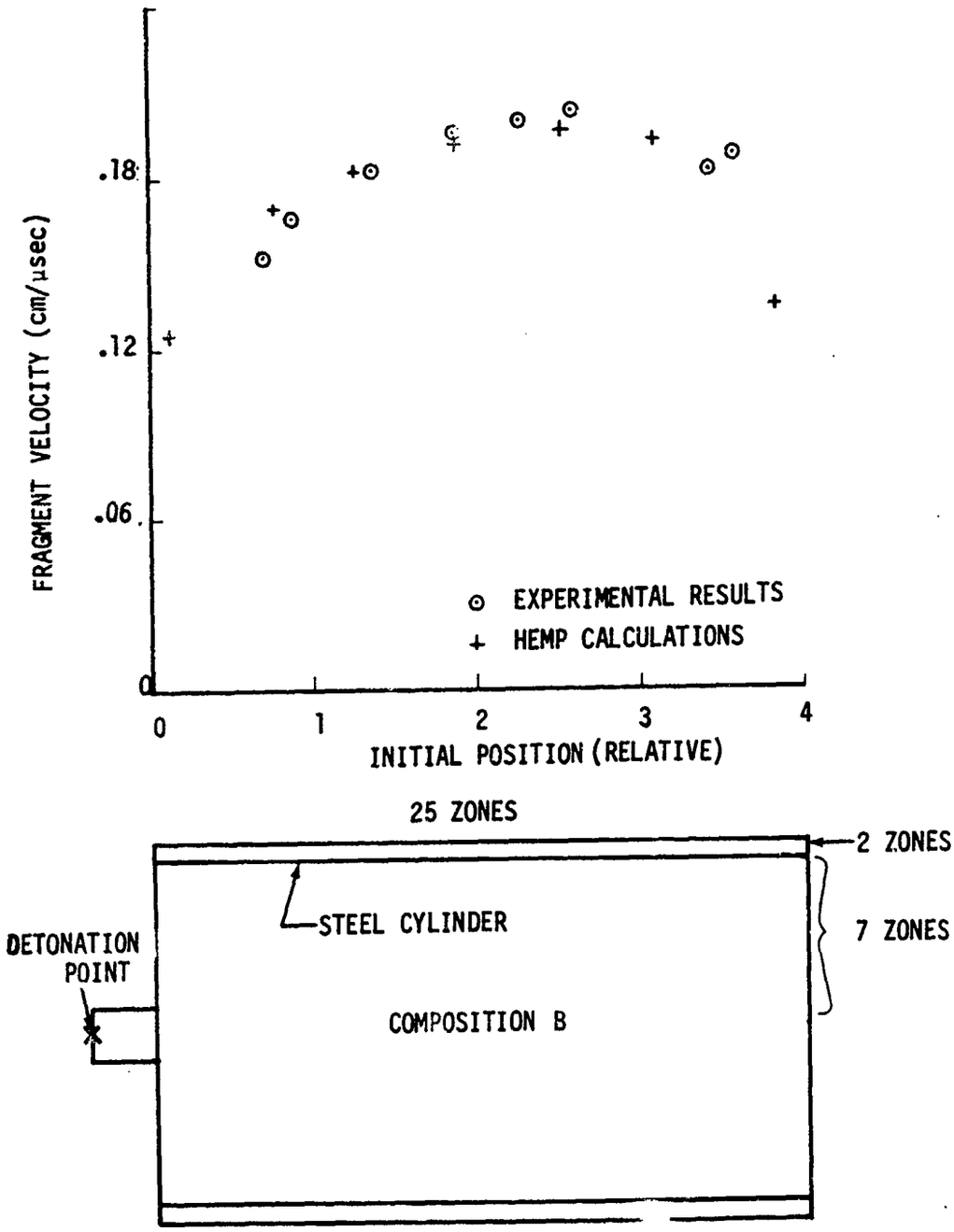

Figure 13. Calculated and experimental results for the speed distribution of fragments propelled from an explosively loaded cylinder

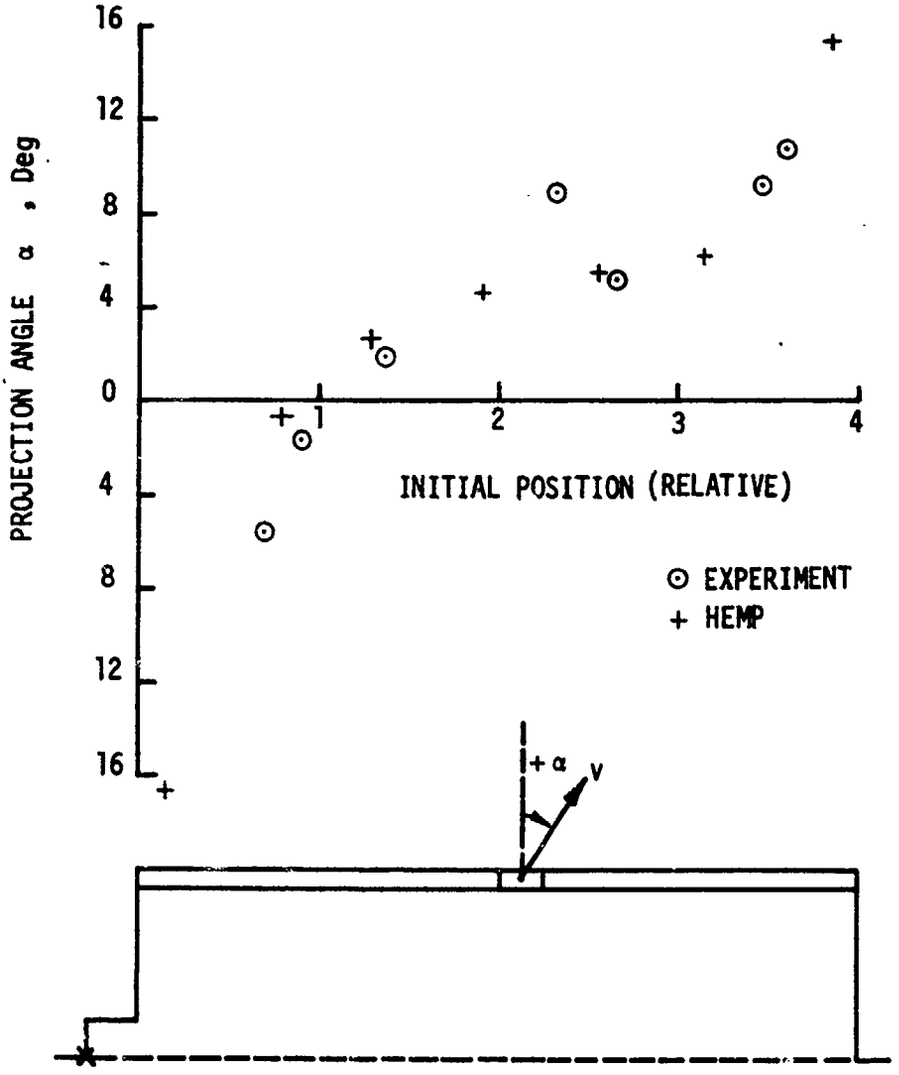

Figure 14. Calculated and experimental results for projection angle distribution of fragments propelled from an explosively loaded cylinder

position B is detonated at one end and the resulting fragment velocities are both measured and calculated. In the calculations, the steel is considered as an elastic-perfectly plastic solid up to the point of expansion where the pressure becomes less than a predetermined minimum value. From that point on, the steel is treated as a hydrodynamic material in an attempt to model the fragmented liner. The calculations were stopped when it was observed that the velocities of the steel liner had stabilized (about 45 μsec after initiation). The experimental fragment velocities were measured from fragment positions obtained at 300 μsec and at 600 μsec. These velocities are compared in Figure 13 as a function of the initial position along the cylinder. Figure 14 compares the calculated and observed fragment projection angles. Figures 13 and 14 indicate good agreement between calculated and experimental results.

Figures 15, 16 and 17 show the final comparison between calculated and experimental results. The top portions of these photographs show flash radiographs of the event while the lower portions show the calculated configurations. The explosive-metal system consists of a spherical cap of mild steel in contact with a cylindrical explosive (Composition B) and a booster. The metal is accelerated from the left face of the explosive which is initiated on the right end of the booster. Figures 15, 16 and 17 show various stages of the acceleration process to the point where the numerical solution could not be continued without rezoning. In these figures, the relative horizontal location of both the radiographs and the calculated grid is correct. The last comparison (31.8μsec) shows the configuration after the liner has moved about one and a half calibers. The difference between the calculated velocity at this time and velocities estimated from the radiographs is 6 1/2%. For this series of calculations, the JWL equation of state was used to describe the explosive products.[4] The liner material was modeled as an elastic-perfectly plastic material with an equation of a state of the Mie-Grüneisen form. To simulate the edge spall which occurs in the liner, a failure criterion based upon pressure was used. If the pressure in a zone goes below a minimum value (-10Kb), the material in

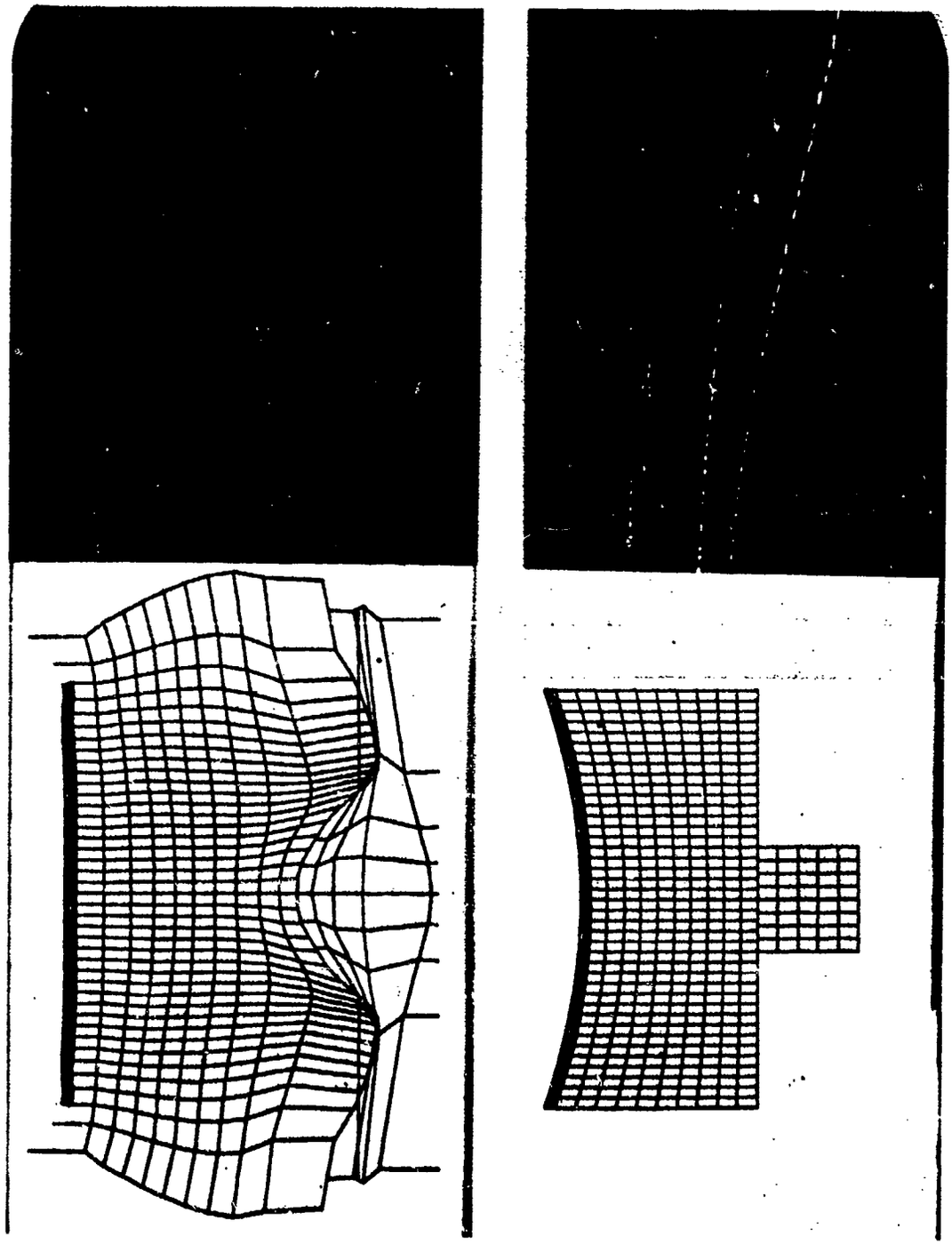

Figure 15. Calculated and experimental configuration of a steel spherical cap accelerated by an incontact explosive at the instant of initiation (right) and 7 μsec after initiation (left)

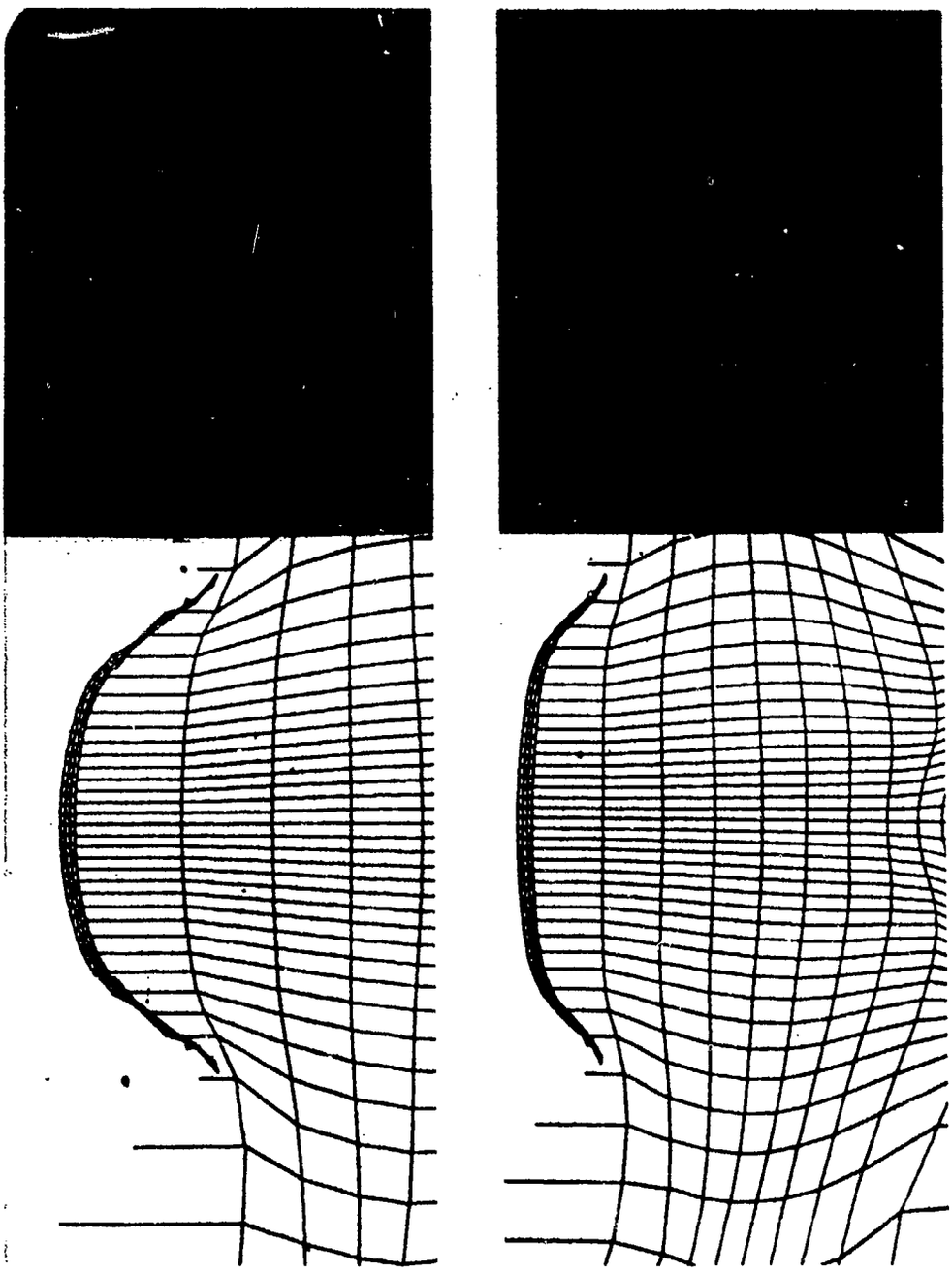

Figure 16. Calculated and experimental configuration of a steel spherical cap accelerated by an incontact explosive at 12.5 μsec (right) and 17.5 μsec (left) after initiation

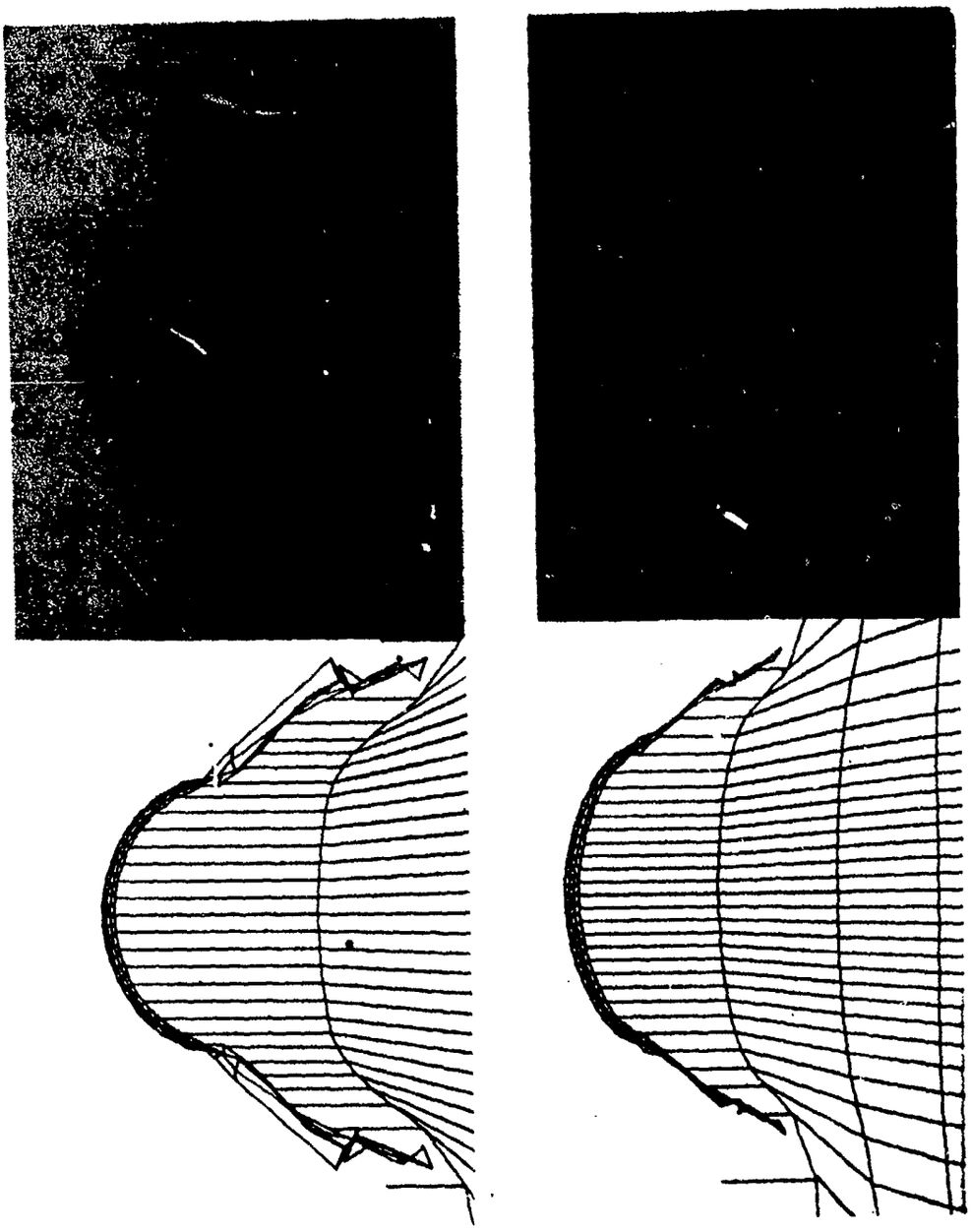

Figure 17. Calculated and experimental configuration of a steel spherical cap accelerated by an incontact explosive at 22.5 μsec (right) and 31.8 μsec (left) after initiation

that zone is considered failed, and the yield strength and shear modulus are set to zero in that zone for the remainder of the calculation. Also, the subsequent pressure in that zone is not allowed to become negative. At 12.5 μsec, spalling of the edges of the liner is apparent in the radiograph. It is also indicated in the calculation by the severely distorted zones. In the calculations, all materials are forced to remain continuous; therefore, spalled regions are indicated by grossly distorted zones, see Figure 17. In order to continue these calculations to 31 μsec, it was necessary to disregard the time step calculation for the spalled zones. The calculated motion of the remainder of the grid should be valid.

IV. SUMMARY AND CONCLUSIONS

In an attempt to gain an understanding of the accuracy obtained from the HEMP code, five problems were solved numerically with it, and these solutions were compared with the exact solutions to the same problems. These problems were selected because they exercised the subroutines which are necessary to solve problems of metal liners accelerated by high explosives. Based upon this comparison the numerical technique appears to generate solutions which agree reasonably with the exact solutions. Problems which are inherently two-dimensional require a finer zoning than one-dimensional problems, if the same quality of solution is desired. Generally, if a coarse zoning is used, structure which appears in the exact solution tends to be smoothed and numerical values may tend to oscillate about the correct values. Also, solutions to problems which are essentially hydrodynamic flows appear to be better than solutions to elastic or elastic-plastic motions.

Four problems which involve the acceleration of metallic liners by high explosives were solved numerically with the HEMP code and these results were compared with experimental observations. In all cases, including the case of preformed fragments, the results were in

reasonable agreement. In calculating the motion of thin liners, it is practical to use only a few mesh zones across the liner thickness. Therefore, no attempt is made to resolve wave motion or stresses in the metal liner; however, based upon the above results, the gross motion of the liner is calculated reasonably well.

From the above comparisons, we conclude that BRL's current version of the HEMP code is operating correctly and that the accuracy is sufficient to make it useful. This code should be applied to current design problems which involve metal liners accelerated by detonating explosives in order to determine if the number of iterations required by current trial and error design techniques can be significantly reduced.

ACKNOWLEDGEMENTS

A version of the HEMP code was obtained from the Lawrence Radiation Laboratory, B division (group headed by M. L. Wilkins) by E. Roecker and G. H. Jonas in December 1967. The code was made functional at BRL by G. H. Jonas and L. Butler. The author received a correct, running version of the code from G. H. Jonas in April 1970. Experimental data for Figure B-11 were obtained by J. Kineke and C. West. Experimental data for Figures B-13 - B-17 were obtained by S. Kronman and R. Gross.

REFERENCES

1. Mark L. Wilkins, "Calculation of Elastic-Plastic Flow, University of California, Lawrence Radiation Laboratory, Report UCRL-7322, Rev. I, Jan 24, 1969.

2. Mark L. Wilkins, "Calculation of Elastic-Plastic Flow", in Methods of Computational Physics, Vol. 3, edited by Alder, B., Fernbach, S., and Rotenburg, M., Academic Press, New York and London, 1964.

3. G. E. Duvall and G. R. Fowles, "Shock Waves" in High Pressure Physics and Chemistry, edited by R. S. Bradley, Chapter 9, Vol. 2, Academic Press, New York, 1963.

4. E. L. Lee, H. C. Hornig, and J. W. Kury, "Adiabatic Expansion of High Explosive Detonation Products", University of California, Lawrence Radiation Laboratory, Report UCRL-50422, May 2, 1968.

5. B. C. Taylor, "Effects of Boundary Rarefactions on Impulse Delivered by Explosive Charge", Third Symposium on Detonation, p.267, Princeton University, Sept. 1960.

6. T. E. Sterne, "A Note on the Initial Velocities of Fragments from Warheads," BRL Report No. 648, Sept. 1947.

7. G. I. Taylor, "The Dynamics of the Combustion Products Behind Plane and Spherical Detonation Fronts in Explosives", Proc. Roy Soc. A200,1061, p. 235-47, 1950.

APPENDIX A
PROBLEM FORMULATION OF THE HEMP CODE

NOTATION:
(All tensors are referred to a fixed Cartesian coordinate system.)

e	specific internal energy
$\dot{\varepsilon}_{ij}$	components of the rate of strain tensor
$\dot{e}_{ij}$	components of the deviator of $\dot{\varepsilon}_{ij}$
G	shear modulus
P	pressure
S_{ij}	components of the deviator of σ_{ij}
t	time
v_i	components of velocity
σ_{ij}	components of the Eulerian stress tensor
σ_Y	yield strength in simple tension
$\frac{D}{Dt}$	material derivative
$\frac{DS}{Dt}_{ij}$	deviator stress rate (Jaumann derivative)
λ	factor of proportionality
ρ	density
$()^p$	implies plastic part
$()^e$	implies elastic part
δ_{ij}	Kronecker delta

A description of the problem formulation and numerical technique used in the HEMP code can be found in references 1 and 2. A brief description is included here for easy reference.

The conservation equations of mass, momentum, and energy may be written with reference to a fixed Cartesian coordinate system as

$$\frac{D\rho}{Dt} + \rho v_{i,i} = 0 \quad , \tag{A.1}$$

$$\rho \frac{Dv_i}{Dt} = \sigma_{ij,j} \quad , \tag{A.2}$$

$$\rho \frac{De}{Dt} = \sigma_{ij}\dot{\varepsilon}_{ij} \quad , \tag{A.3}$$

where the standard convention of summation on repeated subscripts is implied and a comma indicates partial differentiation with respect to that space coordinate. The stain rate is defined as

$$\dot{\varepsilon}_{ij} = \frac{1}{2}(v_{i,j} + v_{j,i}) \, . \tag{A.4}$$

For the plasticity theory used in the code, the strain rate is assumed to be composed of an elastic and a plastic part according to

$$\dot{\varepsilon}_{ij} = \dot{\varepsilon}^{e}_{ij} + \dot{\varepsilon}^{p}_{ij} \, . \tag{A.5}$$

The strain rate deviator, $\dot{e}_{ij}$, is defined by

$$\dot{e}_{ij} = \dot{\varepsilon}_{ij} - \frac{1}{3}\delta_{ij}\dot{\varepsilon}_{kk} \tag{A.6}$$

with similar definitions for the elastic, $\dot{e}^{e}_{ij}$, and plastic, $\dot{e}^{p}_{ij}$, deviators. The stress deviator, S_{ij}, and pressure, P, are given by

$$S_{ij} = \sigma_{ij} + S_{ij}\, P, \qquad P = -\frac{1}{3}\,\sigma_{kk}. \tag{A.7}$$

The von Mises yield function, f, where

$$f = \frac{1}{2}\, S_{ij}\, S_{ij} - \frac{1}{3}\sigma_y^2 \ , \tag{A.8}$$

is used to determine if the material is in an elastic or a plastic state. If $f < 0$ or $f = 0$ and $\frac{df}{dt} < 0$, then the material is in the elastic state and the above equations are supplemented by an equation of state

$$P = P(\rho, e) \ , \tag{A.9}$$

and

$$\frac{DS_{ij}}{Dt} = 2G\dot{e}^{e}_{ij} \ , \qquad \dot{\varepsilon}^{p}_{ij} = 0. \tag{A.10}$$

If $f = 0$ and $\frac{df}{dt} > 0$, then the material is in the plastic state and the preceding relations [(A.1) to (A.8)] are supplemented by

$$P = P(\rho, e) \ , \qquad \frac{DS_{ij}}{Dt} = 2G\dot{e}^{e}_{ij} \ ,$$

$$\dot{e}^{p}_{ij} = \lambda S_{ij} \ , \qquad \dot{\varepsilon}^{p}_{kk} = 0. \tag{A.11}$$

The above system of equations is integrated in time by using an explicit, finite-difference technique. The derivatives appearing in the differential equations are replaced by finite-difference approximations as follows:

a. material derivative

$$\frac{D}{Dt} f_o \sim \frac{f_o(t+\Delta t) - f_o(t)}{\Delta t}$$

where the subscript $_o$ indicates a point fixed in the moving material.

b. partial space derivatives

$$\left.\frac{\partial f}{\partial x}\right|_o \sim \frac{1}{A}\left[f_a(Y_1-Y_4) + f_b(Y_2-Y_1) + f_c(Y_3-Y_2) + f_d(Y_4-Y_3)\right] ,$$

where the subscript notation is referred to Figure A-1. Quantities

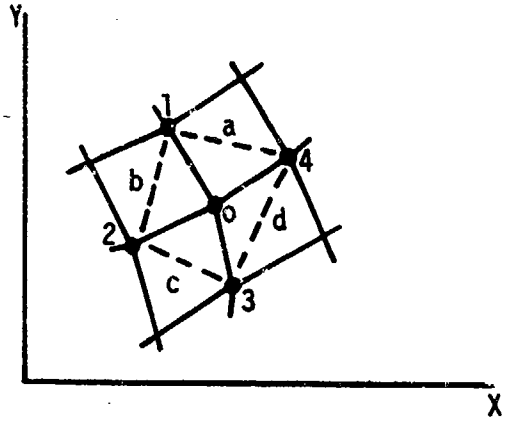

Figure A-1. Finite-Difference Mesh Fixed in Material

like position and velocity are defined at mesh points, but quantities like pressure, volume, etc., are defined at zone centers. In the above equation, f is a zone center quantity and A is the area of the dotted polygon. In this formulation, the finite-difference mesh is fixed in and moves with the material. The approximation used above is derived from

$$\overline{\frac{\partial f}{\partial x}} = \frac{1}{A}\oint_c f dY .$$

A similar expression holds for partial derivatives with respect to Y.

c. stress rate

$$\frac{DS_{ij}}{Dt} \sim \left[\frac{1}{\Delta t}\left(S'_{ij}(t+\Delta t) - S'_{ij}(t)\right)\right] ,$$

where the prime indicates that S'_{ij} is referred to a Cartesian coordinate system which translates and rotates with the material. At time t, the primed coordinate system is aligned with the fixed coordinate system.

The above finite-difference equations are used to reduce the partial differential equations to algebraic equations. Then, from known conditions at one time t, the variables can be estimated at time $t + \Delta t$. First, the momentum equations are used to estimate the velocities over the time increment Δt from the conditions given at time t. The coordinate positions at $t + \Delta t$ for the mesh points are determined from these velocities. Volumes at the end of the time increment are determined from the new coordinate positions. The viscous pressure (based upon the von Neumann-Richtmyer method) which is added to the pressure from the equation of state is calculated from

$$q = \frac{C\rho_0 A}{V}\left[\frac{\dot{V}}{V}\right]^2 \quad \text{if} \quad \dot{V} < 0 \qquad \text{or}$$

$$q = 0 \quad \text{if} \quad \dot{V} \geq 0,$$

where $\dot{V}$ is the volumetric rate of change, A is the zone area, and C is a constant. The strain rate is calculated from Equation (A.4) with the known velocities, and the stress rate is calculated from these strains by Equation (A.10). These stresses are then used to check the yield condition, Equation (A.8). If the stresses are within the elastic range, then these values are correct; however, if the material is plastic, these stresses are reduced by multiplying each component by

$$\sqrt{2/3}\,\sigma_Y (S_{ij}S_{ij})^{-\frac{1}{2}}.$$

Thus, the stress state is reduced to fall on the yield surface, and the flow rule of Equation (A.11) is preserved. The density of each zone is calculated from the continuity equation (A.1), and e and P are obtained from the energy equation (A.3) and the equation of state (A.9). A time increment is next calculated based upon the length of time required for a dilatational wave to transverse a zone. All

quantities are now determined at time $t + \Delta t$. This procedure is continually used to produce a solution over the time interval of interest.

The code can treat boundary conditions of either a stress free boundary or a specified velocity on the boundary. Also, to treat problems which involve two materials which slide relative to each-other, a decoupling of grid points on the interface is accomplished in a slide line routine.